Inorganic Chemistry

Article

pubs.acs.org/IC

Effects of Lanthanoid Cations on the First Electronic Transition of Liquid Water Studied Using Attenuated Total Reflection Far-Ultraviolet Spectroscopy: Ligand Field Splitting of Lanthanoid Hydrates in Aqueous Solutions

Takeyoshi Goto,[†] Akifumi Ikehata,*[,†] Yusuke Morisawa,[‡,∥] Noboru Higashi,[§] and Yukihiro Ozaki[‡]

[†]National Food Research Institute, National Agriculture and Food Research Organization (NARO), Tsukuba, Ibaraki 305-8642, Japan

[‡]Department of Chemistry, School of Science and Technology, Kwansei Gakuin University, Sanda, Hyogo 669-1337, Japan

[§]Kurabo Industries Ltd., Shimokida-cho, Neyagawa, Osaka 572-0823, Japan

[∥]Department of Chemistry, School of Science and Engineering, Kinki University, Higashiosaka, Osaka 577-8502, Japan

ABSTRACT: The effects of the lanthanoid cations (Ln^{3+}) on the first electronic transition ($\tilde{A} \leftarrow \tilde{X}$) of liquid water were studied from the attenuated total reflection far-ultraviolet (ATR-FUV) spectra of trivalent Ln^{3+} electrolyte solutions (1 M), except Pm^{3+}. The $\tilde{A} \leftarrow \tilde{X}$ transition energies of the Ln^{3+} electrolyte solutions show a distinct tetrad in their dependence on the number of 4f electrons of the Ln^{3+} cations. For the half occupation period of the 4f electrons, the $\tilde{A} \leftarrow \tilde{X}$ transition energies decrease from La^{3+} ($4f^0$, 8.0375 eV) to Nd^{3+} ($4f^3$, 8.0277 eV) and increase from Sm^{3+} ($4f^5$, 8.0279 eV) to Gd^{3+} ($4f^7$, 8.0374 eV). For the complete occupation period, there are two local minima at Dy^{3+} ($4f^9$, 8.0349 eV) and Yb^{3+} ($4f^{13}$, 8.0355 eV). The $\tilde{A} \leftarrow \tilde{X}$ transition energies of the tetrad nodes (La^{3+}, Gd^{3+}, Ho^{3+} ($4f^{10}$), and Lu^{3+} ($4f^{14}$)) increase slightly, as the nuclear charge increases in accordance with the hydration energies of the Ln^{3+} cations. The energy difference (ΔE) between the $\tilde{A} \leftarrow \tilde{X}$ transition energies and the line between La^{3+} and Lu^{3+} is largest at Nd^{3+} (80.5 cm^{-1}) for the half occupation period and at Dy^{3+} (26.1 cm^{-1}) and Yb^{3+} (24.5 cm^{-1}) for the complete occupation period. The order of magnitude of ΔE is comparable to the ligand field splitting (LFS) of the ground state multiplets of Ln^{3+} complexes. The observed tetrad trend of the $\tilde{A} \leftarrow \tilde{X}$ transition energies of the Ln^{3+} electrolyte solutions across the 4f period reflects the hydration energies of the Ln^{3+} cations and the LFS induced by water ligands.

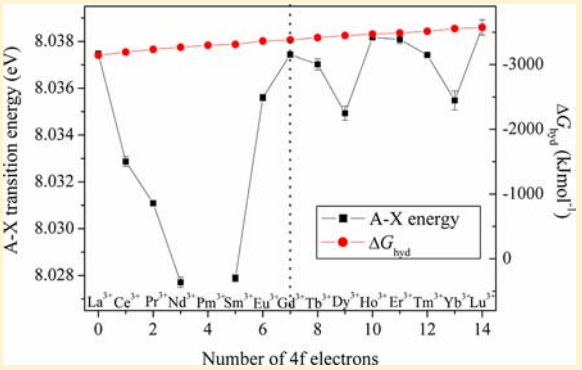

1. INTRODUCTION

The molecular interaction of trivalent lanthanoid cations (Ln^{3+}) with water molecules is important in chemistry and is exploited in many valuable applications, such as Magnetic Resonance Imaging (MRI) contrast agents,[1,2] catalysts,[3,4] and the treatment of nuclear wastes.[5,6] Physicochemical properties of Ln^{3+} hydrates depend on the 4f electron occupation state of the Ln^{3+} cations in the electronic[7,8] and electric aspects.[9] Accordingly, the physicochemical properties of Ln^{3+} hydrates vary across the 4f period in either monotonic or non-monotonic trends. The hydration structure of Ln^{3+} is governed by the electric charge densities of the Ln^{3+} hydrates and the steric hindrance of the water ligands. From computational and X-ray analyses, it was determined that the coordination number of Ln^{3+} hydrates non-monotically decreases from 9 to 8 with a node between Nd^{3+} and Ho^{3+} as the nuclear charge increases,[9−12] while the Ln−OH_2 distances monotonically decrease across the entire 4f period.[13−16] The Gibbs energies of hydration of Ln^{3+} cations increase monotonically as the nuclear charge increases.[17,18] The changes in the partial molar volume,[19] heat capacity,[20] viscosity,[21] and molar Verdet constant[22] of the series of Ln^{3+} aqueous solutions are non-monotonic, and a node is observed around Gd^{3+}. The characteristic tetrad trends of the physicochemical properties of Ln^{3+} hydrates, which depend on the 4f electron occupation state, are known as the tetrad effects.[7,8]

Ligand field splitting (LFS) of Ln^{3+} complexes is relatively small compared to that of transition metal complexes. The splitting of 4f electron energy levels is typically in the order of 10^2 cm^{-1} for LFS, 10^3 cm^{-1} for spin−orbit coupling, and 10^4 cm^{-1} for coulomb interaction; in contrast, the LFS of d electron energy levels is in the order of 10^4 cm^{-1}.[23,24] The 4f electrons of Ln^{3+} complexes are electronically shielded from ligand fields by the outer 5s and 5p electrons.[25,26] The LFS of the ground state multiplets of 4f electrons has been primarily studied on Ln^{3+} ionic crystals using various spectroscopic and computational methods.[27−31] An electronic transition study of $LnCl_6^{3-}$

Received: May 6, 2012
Published: September 24, 2012

   dx.doi.org/10.1021/ic3009255 | *Inorg. Chem.* 2012, 51, 10650−10656

complexes using the valence-bond configuration interaction (VBCI) model indicated that the LFS energy (LFSE) is stabilized by 4f and 3p electron mixing through σ and π interactions between the ligand and the metal orbitals.[32] There have been few studies on the LFS of Ln^{3+} hydrates in aqueous solutions because of the strong optical absorption of the solvent water.[23,33] Vigouroux et al. determined the ground state multiplets of Ln^{3+} hydrates from the longitudinal relaxation rates of the proton of a tetramethylammonium ion in a D_2O solution and showed the tetrad trend of the LFS of Ln^{3+} hydrates across the 4f period.[34] Fries and Belorizky showed that collisions of Ln^{3+} complexes with solvent water molecules modulate the ligand field and govern the electronic relaxation of Ln^{3+} cations.[35]

The first electronic transition ($\tilde{A} \leftarrow \tilde{X}$) of water molecules, which corresponds to the electronic transition from the $(1b_1)^2$ orbital of the ground state ($\tilde{X}^1A_1$) to the ($4a^1$) orbital (n-σ^*) and (3s) Rydberg atomic orbital of the excited state ($\tilde{A}^1B_1$),[36,37] reflects the characteristic hydrogen bonding state of water molecules. The $\tilde{A} \leftarrow \tilde{X}$ transition energy of water is dependent on its physical states: 7.4, 8.2, and 8.4 eV for the vapor,[38] liquid,[39] and solid states,[40] respectively. Owing to the fundamental importance of liquid water in nature, the studies of the $\tilde{A} \leftarrow \tilde{X}$ transition of liquid water have been explicitly developed;[41−44] however, the experimental progress has been limited because of the optically dense property of liquid water. Recently, we developed an attenuated total reflection far-ultraviolet (ATR-FUV) spectroscopic method that enables direct measurement of the electronic transitions of liquid and solid samples.[45−53] Using this method, we reported how the hydrogen bonding state, which is perturbed by temperature changes or the presence of ions, affects the $\tilde{A} \leftarrow \tilde{X}$ transition of liquid water.[50−52] Specifically, the $\tilde{A} \leftarrow \tilde{X}$ transition energy of liquid water increases with decreasing temperature or the addition of salts. The $\tilde{A} \leftarrow \tilde{X}$ transition energies of electrolyte solutions of s- and p-block metal cations linearly correlate with the Gibbs energies of hydration of the cations except the high charge density cations (H^+, Li^+, and Be^{2+}), and the hydration structures of the cations govern the $\tilde{A} \leftarrow \tilde{X}$ transition bandwidth of the electrolyte solutions.[52]

In the present study, the effects of the series of Ln^{3+} cations on the $\tilde{A} \leftarrow \tilde{X}$ transition of liquid water were studied using ATR-FUV spectroscopy to elucidate the electronic nature of Ln^{3+} hydrates in aqueous solutions. ATR-FUV spectra of Ln^{3+} except Pm^{3+} and Group XIII (Al^{3+}, Ga^{3+}, and In^{3+}) metal electrolyte solutions were measured to distinguish the 4f electronic effects on the $\tilde{A} \leftarrow \tilde{X}$ transition of water molecules from the hydration energies of the cations. Then, the $\tilde{A} \leftarrow \tilde{X}$ transition energies of the Ln^{3+} electrolyte solutions were correlated with the number of 4f electrons. From the characterization, the tetrad trend of the $\tilde{A} \leftarrow \tilde{X}$ transition energies across the 4f period was revealed, which reflects the LFS of the 4f electronic states of the Ln^{3+} hydrates.

2. EXPERIMENTAL SECTION

ATR-FUV spectra of electrolyte solutions of Ln^{3+}, except Pm^{3+}, and Group XIII metal cations (Al^{3+}, Ga^{3+}, and In^{3+}) were measured. The same counteranion was used for all the salts to negate the effect of the counteranion on the measured spectra. Nitrate was chosen, since its $\pi-\pi^*$ transition band is well separated from the $\tilde{A} \leftarrow \tilde{X}$ transition band of liquid water. Lanthanum nitrate hexahydrate (purity 99%), cerium nitrate hexahydrate (99%), praseodymium nitrate hexahydrate, neodymium nitrate hexahydrate, samarium nitrate hexahydrate, europium nitrate pentahydrate, gadolinium nitrate hexahydrate, terbium nitrate pentahydrate, dysprosium nitrate hydrate, holmium nitrate pentahydrate, erbium nitrate pentahydrate, thulium nitrate pentahydrate, ytterbium nitrate pentahydrate, lutetium nitrate hydrate, gallium nitrate hydrate, and indium nitrate hydrate were purchased from Sigma-Aldrich Co. (U.S.A.). Aluminum nitrate enneahydrate (98%) was purchased from Kanto Chemical Co., Inc. (Japan). The purity of the metal salts is 99.9% (trace metal basis) unless otherwise indicated. All chemicals were used without further purification. The sample solutions were prepared with deionized water from a Milli-Q system (water resistivity 18.2 MΩcm, TOC 3 ppb, Millipore Corp., U.S.A.).

The details of an ATR-FUV spectrophotometer were previously reported.[46] As a brief overview, the ATR-FUV spectrophotometer is composed of a D_2 lamp (30 W), a monochromator (KV-200, Bunkoh-Keiki Co. Ltd., Japan), a sapphire internal reflection element (IRE), and a photomultiplier tube (PMT) that is equipped with a fused silica plate coated with a sodium salicylate film. The probe light path is continuously purged with N_2 gas (6 L/min) to reduce the FUV light absorption of atmospheric oxygen and water vapor. The incident angle of the probe light is 60° to satisfy a condition for total internal reflection on the aqueous solution-sapphire IRE interface. ATR absorbance is defined as $-\log(I/I_0)$, where I and I_0 are the reflected light intensities of a sample solution and air, respectively. The ATR-FUV spectra of the sample solutions were measured in the range from 145 to 300 nm at 25.0 ± 1.0 °C. The refractive indices at 589.29 nm (n_D) of the sample solutions were measured using a digital refractometer (PAL-BX/RI, Atago Co., Ltd., Japan) at 25.0 ± 1.0 °C. For the current reflectance measurements, the penetration depth of the evanescent wave of the probe light into the aqueous sample phase is about 40 nm.[46] The probe depth is much longer than a single water molecule; therefore the measured ATR-FUV spectra predominantly reflect the molecular information from the interior bulk of the sample solutions.

3. RESULTS AND DISCUSSION

Figure 1a shows the ATR-FUV spectra of pure water and 1 M electrolyte solutions of trivalent metal nitrates. The absorption bands at 5.9896 eV (207.0 nm) and 8.0093 eV (154.8 nm) are assigned to the valence electronic transitions of the nitrate anions ($\pi-\pi^*$)[54] and water molecules ($\tilde{A} \leftarrow \tilde{X}$),[50−52] respectively. The band shapes of the $\tilde{A} \leftarrow \tilde{X}$ transition for the electrolyte solutions differ from that of pure water (Figure 1b). Specifically, the band positions are shifted to a higher energy, and the ATR absorbance decreases for the trivalent cations. Since the counteranion of all the electrolyte solutions is the same nitrate, the observed changes of the $\tilde{A} \leftarrow \tilde{X}$ bands are ascribed to effects of the trivalent cations.

The highly hygroscopic properties and variations in the hydration numbers of the trivalent salts made the sample preparation of electrolyte sample solutions with equal concentrations impractical. For example, in Figure 1, the concentration of all the sample solutions was prepared as 1.0 M, but the ATR absorbance of the nitrate anion at 207 nm varies from 0.177 for the Al^{3+} solution to 0.216 for the Lu^{3+} solution. To compare the effects of the trivalent cations on the $\tilde{A} \leftarrow \tilde{X}$ transition energy, the concentration variations were compensated for by relating the observed $\tilde{A} \leftarrow \tilde{X}$ transition energy with the ATR absorbance of the nitrate anion of each solution. Specifically, the ATR-FUV spectra of four solutions with different concentrations (prepared as 0.75, 1.0, 1.25, and 1.5 M) of each salt were measured, and the $\tilde{A} \leftarrow \tilde{X}$ transition energy was plotted against the ATR absorbance of nitrate anion at 207 nm. Via interpolation with second polynomial fitting for each cation, the value of the $\tilde{A} \leftarrow \tilde{X}$ transition energy at the nitrate anion ATR absorbance of 0.226 was employed as the value for 1 M electrolyte concentration.[54] Figure 2 shows a plot

dx.doi.org/10.1021/ic3009255 | Inorg. Chem. 2012, 51, 10650−10656

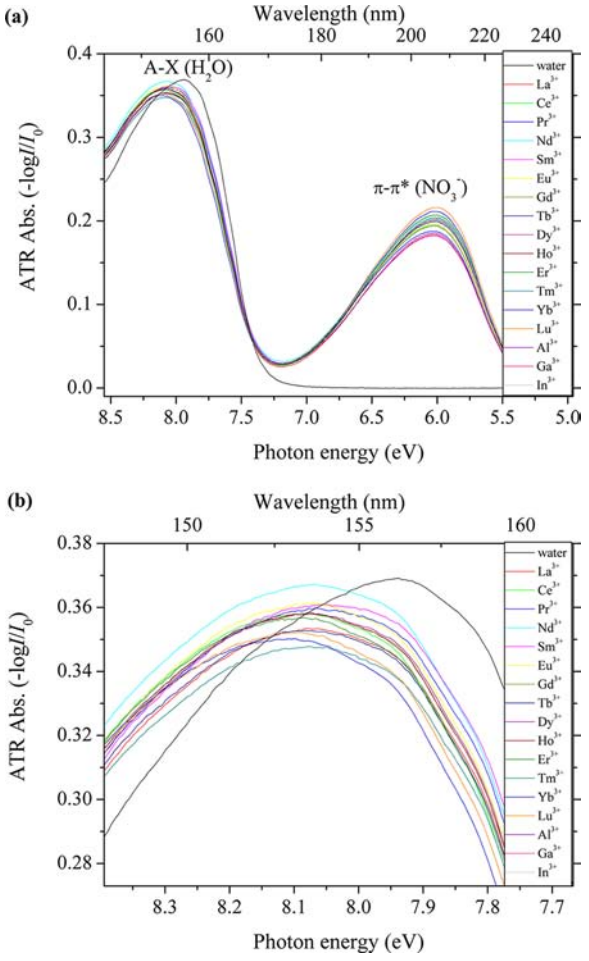

Figure 1. (a) ATR-FUV spectra of pure water and 1 M electrolyte solutions of trivalent metal nitrates. (b) Expanded view of the $\tilde{A} \leftarrow \tilde{X}$ transition bands.

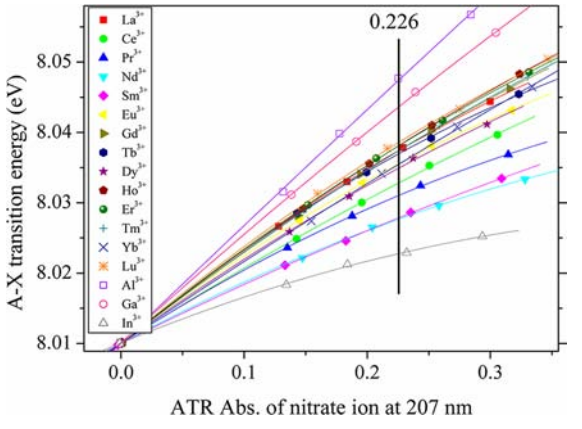

Figure 2. Plot of the $\tilde{A} \leftarrow \tilde{X}$ transition energies versus the ATR absorbance of the nitrate anion at 207 nm for the trivalent electrolyte solutions with the second polynomial fitting curves. The vertical bold line shows the ATR absorbance at 0.226.

of the $\tilde{A} \leftarrow \tilde{X}$ transition energies of the trivalent metal electrolyte solutions against the ATR absorbance of the nitrate anion at 207 nm with second polynomial fitting curves; the vertical bold line shows the ATR absorbance of 0.226. The $\tilde{A} \leftarrow \tilde{X}$ transition energies of the sample solutions were compared using the values of the first moment (the center of mass) of the $\tilde{A} \leftarrow \tilde{X}$ transition bands in the range 7.2084 (172 nm) to 8.5506 eV (145 nm). Similarly, the ATR absorbance of the $\tilde{A} \leftarrow \tilde{X}$ transition bands and the refractive indices of the sample solutions at four different concentrations were plotted against the ATR absorbance of the nitrate anion at 207 nm, and the values at the ATR absorbance of the nitrate anion (0.226) were employed as those for 1 M solutions. The values of the barycenter energies and ATR absorbance of the $\tilde{A} \leftarrow \tilde{X}$ bands for pure water and Ln^{3+} and Group XIII metal cation nitrate electrolyte solutions (1 M) are listed in Table 1.

Table 1. Values of the Barycenter Energies and ATR Absorbance of the $\tilde{A} \leftarrow \tilde{X}$ Bands for Pure Water and Ln^{3+} and Group XIII Metal Cation Nitrate Electrolyte Solutions (1 M)[a]

	barycenter energy (eV)	ATR absorbance
pure water	8.0093	1
La^{3+}	8.0375	0.9529
Ce^{3+}	8.0329	0.9631
Pr^{3+}	8.0311	0.9570
Nd^{3+}	8.0277	0.9699
Sm^{3+}	8.0279	0.9639
Eu^{3+}	8.0356	0.9509
Gd^{3+}	8.0374	0.9418
Tb^{3+}	8.0370	0.9386
Dy^{3+}	8.0349	0.9455
Ho^{3+}	8.0382	0.9544
Er^{3+}	8.0381	0.9365
Tm^{3+}	8.0374	0.9312
Yb^{3+}	8.0355	0.9412
Lu^{3+}	8.0386	0.9290
Al^{3+}	8.0474	0.8588
Ga^{3+}	8.0434	0.9155
In^{3+}	8.0225	0.9727

[a]The ATR absorbance of each solution was normalized with that of pure water.

The $\tilde{A} \leftarrow \tilde{X}$ transition energies of the trivalent metal electrolyte solutions were correlated with the hydration energies of the cations. Figure 3 shows a plot of the $\tilde{A} \leftarrow \tilde{X}$ transition energies of the Ln^{3+} and Group XIII electrolyte solutions (1 M) versus the Gibbs energies of hydration (ΔG_{hyd})

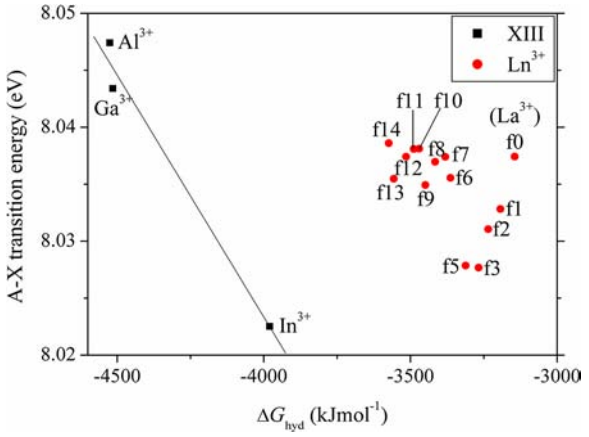

Figure 3. Plot of the $\tilde{A} \leftarrow \tilde{X}$ transition energies of Ln^{3+} and Group XIII electrolyte solutions versus the Gibbs energies of hydration (ΔG_{hyd}) for the corresponding cations.

dx.doi.org/10.1021/ic3009255 | *Inorg. Chem.* 2012, 51, 10650−10656

for the corresponding cations. The experimental values of ΔG_{hyd} were obtained from references 17 and 18 for the Group XIII and Ln^{3+} cations, respectively. The $\tilde{A} \leftarrow \tilde{X}$ transition energies of the Group XIII electrolyte solutions linearly correlate with the ΔG_{hyd} values; this is in agreement with the results from the previous study[52] that showed a linear correlation between the $\tilde{A} \leftarrow \tilde{X}$ transition energies and ΔG_{hyd} values of electrolyte solutions of Group I, II, and XIII cations, except the H^+, Li^+, and Be^{2+} cations, which have a high charge density. Therefore, the hydration energies of the cations correspond to the ground state electronic energy decrease of water molecules of the electrolyte solutions compared to that of pure water, which results in the blue-shift of the $\tilde{A} \leftarrow \tilde{X}$ transition bands. In contrast, the $\tilde{A} \leftarrow \tilde{X}$ transition energies of all the Ln^{3+} electrolyte solutions, including the noble gas-like cation La^{3+} ($[Xe]4f^0$), deviate completely from the linear relation of the Group XIII metal cations. Since the cations in each Group I, II, or XIII (s- and p-block metals) show a linear relationship, the deviation of the Ln^{3+} cations from linearity is attributed to their 4f electronic states.

To investigate the effects of the 4f electronic states on the $\tilde{A} \leftarrow \tilde{X}$ transition energies of the Ln^{3+} electrolyte solutions, the $\tilde{A} \leftarrow \tilde{X}$ transition energies were correlated with the number of 4f electrons. Figure 4 shows a plot of the $\tilde{A} \leftarrow \tilde{X}$ transition energies (filled rectangles, left axis) versus the number of 4f electrons of the Ln^{3+} cations. The error bars of the $\tilde{A} \leftarrow \tilde{X}$ transition energies are derived from the standard deviation of the second polynomial fitting as shown in Figure 2. The dependence of the $\tilde{A} \leftarrow \tilde{X}$ transition energy on the 4f electron occupation state is a tetrad trend; that is, there are four local trends: La^{3+} ($4f^0$) to Nd^{3+} ($4f^3$), Sm^{3+} ($4f^5$) to Gd^{3+} ($4f^7$), Gd^{3+} to Ho^{3+} ($4f^{10}$), and Er^{3+} ($4f^{11}$) to Lu^{3+} ($4f^{14}$); although the value at Pm^{3+} ($4f^4$) was not determined. For the half occupation period of the 4f electrons, the $\tilde{A} \leftarrow \tilde{X}$ transition energies decrease from La^{3+} (8.0375 eV) to Nd^{3+} ($4f^3$, 8.0277 eV) and increase from Sm^{3+} ($4f^5$, 8.0279 eV) to Gd^{3+} (8.0374 eV). For the complete occupation period, there are two local minima at Dy^{3+} ($4f^9$, 8.0349 eV) and Yb^{3+} ($4f^{13}$, 8.0355 eV), and the changes of the $\tilde{A} \leftarrow \tilde{X}$ transition energies are smaller than those of the half occupation period. The $\tilde{A} \leftarrow \tilde{X}$ transition energies at the nodes (La^{3+}, Gd^{3+}, Ho^{3+}, and Lu^{3+}) slightly increase as the nuclear charge increases from La^{3+} (8.0375 eV) through Gd^{3+} (8.0374 eV) and Ho^{3+} (8.0382 eV) to Lu^{3+} (8.0386 eV).

The slight increase of the $\tilde{A} \leftarrow \tilde{X}$ transition energies of the nodes across the 4f period corresponds to an increase in the hydration energies of the Ln^{3+} cations. Since the ΔG_{hyd} values of the Ln^{3+} cations almost linearly correlate with the number of the 4f electron from −3145 kJ/mol for La^{3+} through −3381 kJ/mol for Gd^{3+} to −3574 kJ/mol for Lu^{3+}, as shown in Figure 4 (filled circles, right axis), the ΔG_{hyd} plot can overlap with the line of the $\tilde{A} \leftarrow \tilde{X}$ transition energies between La^{3+} and Lu^{3+}. The $\tilde{A} \leftarrow \tilde{X}$ transition energies of the node species (Gd^{3+} and Ho^{3+}) are located close to the line. Since the $\tilde{A} \leftarrow \tilde{X}$ transition energies and ΔG_{hyd} values of Group I, II, and XIII metal cations are linearly correlated,[52] the $\tilde{A} \leftarrow \tilde{X}$ transition energies of the water molecules hydrating the cations are associated with the hydration energies of the cations in the ground state and in the excited state. Therefore, the primary trend of the $\tilde{A} \leftarrow \tilde{X}$ transition energies of the Ln^{3+} electrolyte solutions is linear with the hydration energies of the Ln^{3+} cations, as shown by the $\tilde{A} \leftarrow \tilde{X}$ transition energies of the node species.

The $\tilde{A} \leftarrow \tilde{X}$ transition energies of the Ln^{3+} cations other than the node species deviate from the hydration energy line in a tetrad trend. To elucidate this energy deviation, the differences between the $\tilde{A} \leftarrow \tilde{X}$ transition energies and the thermodynamic hydration energies were calculated via subtraction. Figure 5 shows a plot of the energy differences (ΔE, filled squares) between the measured $\tilde{A} \leftarrow \tilde{X}$ transition energies and the line between La^{3+} and Lu^{3+} across the 4f period. For the half occupation period, the ΔE increases from La^{3+} to Nd^{3+} (9.98×10^{-3} eV, 80.5 cm^{-1}) and decreases from Sm^{3+} (9.97×10^{-3} eV, 80.4 cm^{-1}) to Gd^{3+} (5.99×10^{-4} eV, 4.83 cm^{-1}). For the complete occupation period, the ΔE shows local maxima at Dy^{3+} (3.24×10^{-3} eV, 26.1 cm^{-1}) and Yb^{3+} (3.03×10^{-3} eV, 24.5 cm^{-1}) and a local minimum in-between Ho^{3+} and Er^{3+}.

The tetrad trend of the ΔE values across the 4f period is mainly ascribed to the effects of LFS on the inner 4f electrons of the Ln^{3+} cations, although the nephelauxetic decrease of the interelectronic repulsion energy of the 4f electrons may contribute to some extent.[7,8] First, the observed ΔE values are on a comparable order of magnitude with the splitting ground state multiplets of Ln^{3+} complexes that are induced by ligand fields, which are mostly in the range 0 to 400 cm^{-1}.[23,27−34,55] Very little information exists on the LFS of

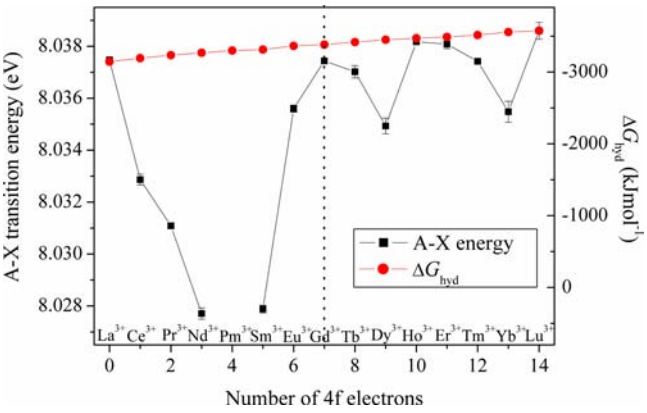

Figure 4. Plot of the $\tilde{A} \leftarrow \tilde{X}$ transition energies (filled squares, left axis) and ΔG_{hyd} values (filled circles, right axis) versus the number of 4f electrons of the Ln^{3+} cations. The error bars of the $\tilde{A} \leftarrow \tilde{X}$ transition energy plot are derived from the standard deviation of the second polynomial fitting error in Figure 2.

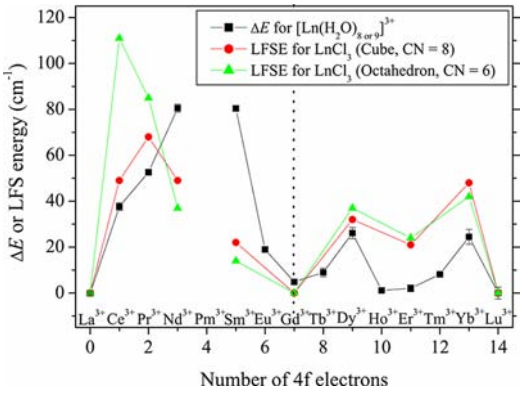

Figure 5. Differences (ΔE, filled squares) between the measured $\tilde{A} \leftarrow \tilde{X}$ transition energies and the line between La^{3+} and Lu^{3+} and the LFS energy of the $LnCl_3$ crystals at the vertices of a cube (CN = 8, filled circles) and an octahedron (CN = 6, filled triangles) from ref 27.

dx.doi.org/10.1021/ic3009255 | Inorg. Chem. 2012, 51, 10650−10656

the ground state multiplets of Ln^{3+} hydrates because of the strong optical absorption of aqueous solvents.[34] From an excited state calculation using the INDO/S−CI method, the split energy is 0 to 263 cm^{-1} for $[Pr(H_2O)_9]^{3+}$ (D_{3h} symmetry) and 0 to 196 cm^{-1} for $[Tm(H_2O)_8]^{3+}$ (D_{2d} symmetry).[33] Second, the observed ΔE profile along the 4f period is more similar to the LFS profile of the ground state multiplets of the cubic geometry (coordination number (CN) = 8) than that of the octahedral geometry (CN = 6) of Ln^{3+} halide crystals. It is thought that the LFS profile is not significantly affected by the difference in the ligand molecules. Yatsimirskii et al. calculated the ground state multiplets of Ln^{3+} halide crystals.[27] The calculated LFS energies for cubic (filled circles) and octahedral (filled triangles) geometries of a $LnCl_3$ crystal are plotted in Figure 5. For all LnX_3 crystals (X = F, Cl, Br, and I), the maximum LFS energy for the half occupation was observed at Ce^{3+} and Pr^{3+} for the octahedral and cubic geometries, respectively. With an increase in the CN of the Ln^{3+} complexes from 6 to 8, the position of the maximum LFS value moves toward the middle of the half occupation period. For the complete occupation period, local maxima are found at Dy^{3+} and Yb^{3+} for both geometries; that is similar to the ΔE profile. The molecular geometry of Ln^{3+} hydrates in aqueous solutions is tricapped trigonal prism (CN = 9) for light elements and square antiprism (CN = 8) for heavy elements.[11,13,14,56] Although the LFS profiles for tricapped trigonal prismatic and square antiprismatic geometries of Ln^{3+} hydrates have not yet been determined, the closer similarity of the ΔE profile with the LFS profile of the cubic (CN = 8) rather than octahedral (CN = 6) geometry of Ln^{3+} halides indicates that the observed tetrad trend of ΔE reflects the LFS of the ground state multiplets of Ln^{3+} hydrates from the perspective of the CN.

The change of the hydration structure around the Ln^{3+} center along the 4f series does not directly contribute to the tetrad trend of the $\tilde{A} \leftarrow \tilde{X}$ transition energies of the Ln^{3+} electrolyte solutions. As the nuclear charge of Ln^{3+} increases, the $Ln^{3+}-OH_2$ distance monotonically decreases along the 4f period. An extended X-ray absorption fine structure (EXAFS) spectroscopic study showed that the $Ln^{3+}-OH_2$ distance in aqueous solution is 2.560 Å for La^{3+}, 2.405 Å for Gd^{3+}, and 2.307 Å for Lu^{3+}.[13] Since the $Ln^{3+}-OH_2$ bond is mostly ionic, the effective charge of the Ln^{3+} cation and the geometric limitations of the coordination sphere primarily govern the structure of the Ln^{3+} hydrate. The hydration number of the Ln^{3+} hydrate gradually shifts from 9 to 8 as the Ln^{3+} cation size decreases.[11,13,14,56] The symmetry of the tricapped trigonal prismatic structure of the Ln^{3+} hydrate distorts from La^{3+} to Gd^{3+} and one capping water is partially lost around Ho^{3+} in the series. The hydrogen bonding state among the water ligands also varies as the nuclear charge increases. From the optimized structures of $[Ln(H_2O)_8]^{3+}$ and $[Ln(H_2O)_9]^{3+}$ complexes calculated by the unrestricted density functional theory (UDFT), the average hydrogen bond length ($r_{O\cdots H}$) monotonically shortens from 2.96 to 2.81 Å and from 2.87 to 2.71 Å, respectively, along the 4f period.[9] As the hydrogen bond length of water molecules is shorter, the increased hydrogen bond donor−acceptor interactions among the water molecules result in the monotonic blue-shift of the $\tilde{A} \leftarrow \tilde{X}$ transition energy of the water molecules.[42,44,52] Thus, the observed tetrad trend of the $\tilde{A} \leftarrow \tilde{X}$ transition energies of the Ln^{3+} electrolyte solutions is not due to variation of the hydration structure along the 4f period but from the splitting of the 4f orbitals of the Ln^{3+} cations by the water ligands.

The zero-point energy differences of the $Ln^{3+}-O$ bonds along the 4f period also do not contribute to the tetrad trend of the $\tilde{A} \leftarrow \tilde{X}$ transition energies of the Ln^{3+} electrolyte solutions. The vibrational energies of the $Ln^{3+}-H_2O$ bond (ν_{M-O}) monotonically increase across the 4f period: An infrared spectroscopic study showed that the ν_{M-O} bands of $Ln(H_2O)_9(C_2H_5SO_4)_3$ crystals are monotonically shifted from 316 cm^{-1} (La^{3+}) to 342 cm^{-1} (Lu^{3+}).[57]

The tetrad trend across the 4f period was also observed for the ATR absorbance of the $\tilde{A} \leftarrow \tilde{X}$ transition bands of the Ln^{3+} electrolyte solutions. Specifically, the ATR absorbance of the half occupation period of the 4f electrons is distinctly larger than that of the complete occupation period. Figure 6 shows a plot of the ATR absorbance (filled rectangles, left axis), which is normalized with that of pure water, and the refractive indices (filled circles, right axis) of the Ln^{3+} electrolyte solutions versus the number of 4f electrons. For both the ATR absorbance and the refractive indices, the values for the 1 M electrolyte solutions were determined via interpolation of the second polynomial fits of the ATR absorbance of the nitrate anion at 207 nm similar to the method used to determine the $\tilde{A} \leftarrow \tilde{X}$ transition energy. The error bar is derived from the standard deviation of the polynomial fitting from the ATR absorbance of the nitrate anion. The ATR absorbance of the Ln^{3+} electrolyte solutions is lower than that of pure water in accordance with the increase in the refractive indices from 1.328 (pure water) to ~1.369. For the half occupation period, the normalized ATR absorbance increases from La^{3+} (0.9529) to Nd^{3+} (0.9699) and then decreases to Gd^{3+} (0.9418). For the complete occupation period, two local maxima exist at Ho^{3+} (0.9544) and Yb^{3+} (0.9412). Since a tetrad trend was observed for the n_D values, it is expected that the tetrad trend of the ATR absorbance is at least partially due to the real part of the refractive indices of the sample solutions. The absorption coefficients were determined by applying Kramers−Kronig transformation (KKT) to the measured ATR spectra to determine the electronic transition probability of each trivalent electrolyte solution; however, the observed differences in the ATR absorbance were too small to verify the KKT calculation results.

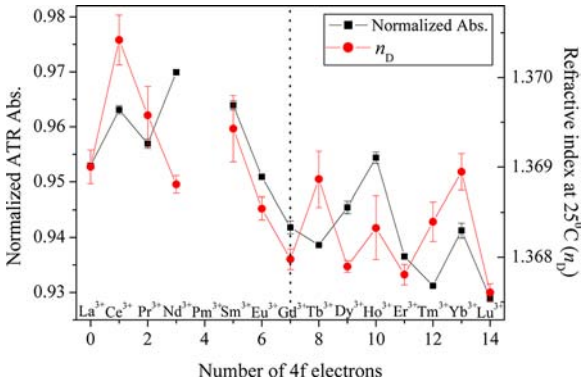

Figure 6. Plot of the ATR absorbance (filled squares, left axis) and the refractive indices (filled circles, right axis) of 1 M Ln^{3+} electrolyte solutions versus the number of 4f electrons. The error bars are derived from the standard deviation of the second polynomial fitting error against the ATR absorbance of the nitrate anion.

The observed tetrad dependence of the ATR absorbance might reflect the degree of charge transfer (CT) interactions between the Ln^{3+} cations and water ligands. The Ln−O bond is predominantly an electrostatic and CT interaction[9] with very

dx.doi.org/10.1021/ic3009255 | Inorg. Chem. 2012, 51, 10650−10656

weak covalent interactions.[58] The degree of CT interactions in Ln^{3+} hydrates is evaluated from the bond length differences between the crystallographic distance measured by X-ray diffraction and the Ln^{3+}–O distance measured via X-ray absorption spectroscopy. The bond length difference is maximized at the half occupation period and becomes small at the middle of the 4f period.[59,60] Thus, the degree of the electron donation from the water ligands to the Ln^{3+} cations depends on the 4f electron occupation state similarly to the observed trend of the ATR absorbance.

4. CONCLUSIONS

This study investigated the effects of Ln^{3+} cations on the $\tilde{A} \leftarrow \tilde{X}$ transition of liquid water using ATR-FUV spectroscopy. ATR-FUV spectra of nitrate electrolyte solutions of the Ln^{3+} cations, except Pm^{3+} and Group XIII metal cations (Al^{3+}, Ga^{3+}, and In^{3+}), were measured. Although the $\tilde{A} \leftarrow \tilde{X}$ transition energies of the Group XIII metal electrolyte solutions linearly correlate with the Gibbs energies of hydration of the cations, those of the Ln^{3+} electrolyte solutions, including the noble gas–like cation La^{3+} ($[Xe]4f^0$), deviate from the linear relation because of the effects of the 4f electronic states. Characterization of the $\tilde{A} \leftarrow \tilde{X}$ transition energies of the Ln^{3+} electrolyte solutions revealed a tetrad trend along the 4f period that results from the LFS of the ground state multiplets of the Ln^{3+} hydrates. As the nuclear charge increases across the 4f period, the $\tilde{A} \leftarrow \tilde{X}$ transition energies at the tetrad nodes slightly increase from La^{3+} (8.0375 eV) through Gd^{3+} (8.0374 eV) and Ho^{3+} (8.0382 eV) to Lu^{3+} (8.0386 eV), which corresponds to the increase in the hydration energies of the cations. The difference (ΔE) between the $\tilde{A} \leftarrow \tilde{X}$ transition energies and the line between La^{3+} and Lu^{3+} has a maximum between Nd^{3+} (9.98×10^{-3} eV, 80.5 cm^{-1}) and Sm^{3+} (9.97×10^{-3} eV, 80.4 cm^{-1}) for the half occupation period and two local maxima at Dy^{3+} (3.24×10^{-3} eV, 26.1 cm^{-1}) and Yb^{3+} (3.03×10^{-3} eV, 24.5 cm^{-1}) for the complete occupation period. The values of ΔE were on a comparable order to the LFS of the ground state multiplets of Ln^{3+} complexes. Consequently, the observed tetrad trend of the $\tilde{A} \leftarrow \tilde{X}$ transition energies across the 4f period reflects the hydration energies of the Ln^{3+} cations and the LFS induced by the water ligands. The ATR absorbance of the $\tilde{A} \leftarrow \tilde{X}$ transition bands of the Ln^{3+} electrolyte solutions also showed a tetrad trend across the 4f period and is larger for the half occupation period than for the complete occupation period. The degree of charge transfer interactions between the Ln^{3+} cations and water ligands might govern the observed tetrad trend of the ATR absorbance.

AUTHOR INFORMATION

Corresponding Author

*E-mail: ikehata@affrc.go.jp.

Notes

The authors declare no competing financial interest.

ACKNOWLEDGMENTS

This work was supported by the System Development Program for Advanced Measurement and Analysis (Program-S) of the Japan Science and Technology Agency (JST).

REFERENCES

(1) H. Kato, H.; Kanazawa, Y.; Okumura, M.; Taninaka, A.; Yokawa, T.; Shinohara, H. *J. Am. Chem. Soc.* **2003**, *125*, 4391.

(2) Aime, S.; Barge, A.; Castelli, D. D.; Fedeli, F.; Mortillaro, A.; Nielsen, F. U.; Terreno, E. *Magn. Reson. Med.* **2002**, *47*, 639.

(3) Kluger, R.; Cameron, L. L. *J. Am. Chem. Soc.* **2002**, *124*, 3303.

(4) Forsberg, J. H.; Spaziano, V. T.; Balasubramanian, T. M.; Liu, G. K.; Kinsley, S. A.; Duckworth, C. A.; Poteruca, J. J.; Brown, P. S.; Miller, J. L. *J. Org. Chem.* **1987**, *52*, 1017.

(5) Gruner, B.; Plesek, J.; Baca, J.; Cısarova, I.; Dozol, J. F.; Rouquette, H.; Vinas, C.; Selucky, P.; Rais, J. *New J. Chem.* **2002**, *26*, 1519.

(6) Salanne, M.; Simon, C.; Turq, P.; Madden, P. A. *J. Phys. Chem. B* **2008**, *112*, 1177.

(7) Jørgensen, C. K. Spectroscopy of Transition-Group Complexes. In *Advances in Chemical Physics*; Prigogine, I., Ed.; John Wiley & Sons, Inc.: Hoboken, NJ; 2007; Vol. *5*; Chapter 2.

(8) Nugent, L. J. *J. Inorg. Nucl. Chem.* **1970**, *32*, 3485.

(9) Kuta, J.; Clark, A. E. *Inorg. Chem.* **2010**, *49*, 7808.

(10) Duvail, M.; Spezia, R.; Vitorge, P. *Chem. Phys. Chem.* **2008**, *9*, 693.

(11) Ciupka, J.; Cao-Dolg, X.; Wiebke, J.; Dolg, M. *Phys. Chem. Chem. Phys.* **2010**, *12*, 13215.

(12) Buzko, V.; Sukhno, I.; Polushin, A.; Kashaev, D. *Int. J. Quantum Chem.* **2011**, *111*, 2705.

(13) Persson, I.; D'Angelo, P.; De Panfilis, S.; Sandström, M.; Eriksson, L. *Chem.—Eur. J.* **2008**, *14*, 3056.

(14) Seitz, M.; Oliver, A. G.; Raymond, K. N. *J. Am. Chem. Soc.* **2007**, *129*, 11153.

(15) Allen, P. G.; Bucher, J. J.; Shuh, D. K.; Edelstein, N. M.; Craig, I. *Inorg. Chem.* **2000**, *39*, 595.

(16) Johansson, G.; Wakita, H. *Inorg. Chem.* **1985**, *24*, 3047.

(17) Marcus, Y. *J. Chem. Soc., Faraday Trans.* **1991**, *87*, 2995.

(18) Goldman, S.; Morss, L. R. *Can. J. Chem.* **1975**, *53*, 2695.

(19) Spedding, F. H.; Pikal, M. J.; Ayers, B. O. *J. Phys. Chem.* **1966**, *70*, 2440.

(20) Spedding, F. H.; Jones, K. C. *J. Phys. Chem.* **1966**, *70*, 2450.

(21) Spedding, F. H.; Pikal, M. J. *J. Phys. Chem.* **1966**, *70*, 2430.

(22) Miyamoto, K.; Isai, K.; Suwa, M.; Watarai, H. *J. Am. Chem. Soc.* **2009**, *131*, 6328.

(23) William, T. C. The Absorption and Fluorescence Spectra of Rare Earth Ions in Solution. In *Handbook on the Physics and Chemistry of Rare Earths*; Gschneidner, K. A., Jr., Eyring, L., Eds.; North-Holland Publishing Company: Amsterdam, The Netherlands, 1979; Vol. *3*, Chapter 24.

(24) Beitz, J. V. Similarities and Differences in Trivalent Lanthanide- and Actinide-Ion Solution Absorption Spectra and Luminescence Studies. In *Handbook on the Physics and Chemistry of Rare Earths*; Gschneidner, K. A., Jr., Eyring, L., Choppin, G. R., Lander, G. H., Eds.; North-Holland Publishing Company: Amsterdam, The Netherlands, 1994; Vol. *18*, Chapter 120.

(25) Goldschmid, Z. B. Atomic Properties (Free Atom). In *Handbook on the Physics and Chemistry of Rare Earths*; Gschneidner, K. A., Jr., Eyring, L., Eds.; North-Holland Publishing Company: Amsterdam, The Netherlands, 1978; Vol. *1*, Chapter 1.

(26) Burns, G. *Phys. Rev.* **1962**, *128*, 2121.

(27) Yatsimirskii, K. B.; Kostromina, N. A. *Theor. Exp. Chem.* **1966**, *2*, 436.

(28) Richardson, F. S.; Reid, M. F.; Dallara, J. J.; Smith, R. D. *J. Chem. Phys.* **1985**, *83*, 3813.

(29) Ishikawa, N.; Sugita, M.; Okubo, T.; Tanaka, N.; Iino, T.; Kaizu, Y. *Inorg. Chem.* **2003**, *42*, 2440.

(30) Zbiri, M.; Atanasov, M.; Daul, C.; Garcia-Lastra, J. M.; Wesolowski, T. A. *Chem. Phys. Lett.* **2004**, *397*, 441.

(31) Hölsä, J.; Karppinen, M.; Kestilä, E. *J. Alloys Compd.* **1994**, *207–208*, 65.

(32) Atanasov, M.; Daul, C.; Güdel, H. U.; Wesolowski, T. A.; Zbiri, M. *Inorg. Chem.* **2005**, *44*, 2954.

(33) Kotzian, M.; Fox, T.; Rosch, N. *J. Phys. Chem.* **1995**, *99*, 600.

(34) Vigouroux, C.; Belorizky, E.; Fries, P. H. *Eur. Phys. J. D* **1999**, *5*, 243.

(35) Fries, P. H.; Belorizky, E. *J. Chem. Phys.* **2012**, *136*, 074513.

(36) Mulliken, R. S. *J. Chem. Phys.* **1935**, *3*, 506.
(37) Herzberg, G. In *Molecular Spectra and Molecular Structure III: Electronic Spectra and Electronic Structure of Polyatomic Molecules*, 2nd ed.; Van Nostrand: New York, 1966; Chapter 5.
(38) Watanabe, K.; Zelikoff, M. *J. Opt. Soc. Am.* **1953**, *43*, 753.
(39) Quickenden, T. I.; Irvin, J. A. *J. Chem. Phys.* **1980**, *72*, 4416.
(40) Onaka, R.; Takahashi, T. *J. Phys. Soc. Jpn.* **1968**, *24*, 548.
(41) Quickenden, T. I.; Irvin, J. A. *J. Chem. Phys.* **1980**, *72*, 4416.
(42) Cabral do Couto, P.; Chipman, D. M. *J. Chem. Phys.* **2010**, *132*, 244307.
(43) Houee-Levin, C.; Tannous, C.; Jay-Gerin, J. P. *J. Phys. Chem.* **1989**, *93*, 7074.
(44) Chipman, D. M. *J. Chem. Phys.* **2005**, *122*, 044111.
(45) Ozaki, Y.; Morisawa, Y.; Ikehata, A.; Higashi, N. *Appl. Spectrosc.* **2012**, *1*, 1.
(46) Higashi, N.; Ikehata, A.; Ozaki, Y. *Rev. Sci. Instrum.* **2007**, *78*, 103107.
(47) Morisawa, Y.; Ikehata, A.; Higashi, N.; Ozaki, Y. *J. Phys. Chem. A* **2011**, *115*, 562.
(48) Morisawa, Y.; Ikehata, A.; Higashi, N.; Ozaki, Y. *Chem. Phys. Lett.* **2009**, *476*, 205.
(49) Tachibana, S.; Morisawa, Y.; Ikehata, A.; Sato, H.; Higashi, N.; Ozaki, Y. *Appl. Spectrosc.* **2011**, *65*, 221.
(50) Ikehata, A.; Higashi, N.; Ozaki, Y. *J. Chem. Phys.* **2008**, *129*, 234510.
(51) Ikehata, A.; Mitsuoka, M.; Morisawa, Y.; Kariyama, N.; Higashi, N.; Ozaki, Y. *J. Phys. Chem. A* **2010**, *114*, 8319.
(52) Goto, T.; Ikehata, A.; Morisawa, Y.; Higashi, N.; Ozaki, Y. *Phys. Chem. Chem. Phys.* **2012**, *14*, 8097.
(53) Higashi, N.; Ikehata, A.; Kariyama, N.; Ozaki, Y. *Appl. Spectrosc.* **2008**, *62*, 1022.
(54) Maria, H. J.; McDonald, J. R.; McGlynn, S. P. *J. Am. Chem. Soc.* **1973**, *95*, 1050.
(55) Zbiri, M.; Daul, C. A.; Wesolowski, T. A. *J. Chem. Theory Comput.* **2006**, *2*, 1106.
(56) Kowall, T.; Foglia, F.; Helm, L.; Merbach, A. E. *J. Phys. Chem.* **1995**, *99*, 13078.
(57) Yamauchi, S.; Kanno, H.; Akama, Y. *Chem. Phys. Lett.* **1988**, *151*, 315.
(58) Lewis, W. B.; Jackson, J. A.; Lemons, J. F.; Taube, H. *J. Chem. Phys.* **1962**, *36*, 694.
(59) David, F. H.; Vokhmin, V. *J. Phys. Chem. A* **2001**, *105*, 9704.
(60) David, F. H. *Radiochim. Acta* **2008**, *96*, 135.